Macromolecular Nanotechnology

# Mechanical properties of attapulgite clay reinforced polyurethane shape-memory nanocomposites

Bin Xu [a], W.M. Huang [b], Y.T. Pei [c], Z.G. Chen [c], A. Kraft [a], R. Reuben [a], J.Th.M. De Hosson [c], Y.Q. Fu [a,*]

[a] Department of Mechanical Engineering, School of Engineering and Physical Sciences, Heriot-Watt University, Edinburgh EH14 4AS, UK
[b] School of Mechanical and Aerospace Engineering, Nanyang Technological University, 50 Nanyang Avenue, 639798, Singapore
[c] Department of Applied Physics, Materials Innovation Institute M2i, University of Groningen, Nijenborgh 4, 9747 AG Groningen, The Netherlands

## ARTICLE INFO

## ABSTRACT

Nanocomposites based on attapulgite clay and shape-memory polyurethane were fabricated by mechanical mixing. The mechanical properties of samples were evaluated using a micro-indentation tester. The untreated commercial attapulgite clay resulted in a significant decrease in glass transition temperature and hardness of the nanocomposite due to the presence of moisture as well as the clay's amorphous structure and surface hydroxyl groups. The attapulgite nanoparticles were heat-treated at 850 °C, which resulted in crystallization of the particles and formation of layered attapulgite structure. The hardness of the nanocomposites composed of the heat treated clay powder dramatically increased as a function of clay content, which is attributed to the homogeneous dispersion of the nanofillers in the polymer matrix and strong filler–polymer interactions. Shape recovery of indentations has been demonstrated upon heating.

© 2009 Elsevier Ltd. All rights reserved.

## 1. Introduction

Recently, organic–inorganic nanocomposites have attracted considerable attention for the enhanced performance in mechanical, electrical, optical and other functional properties [1–4]. The polymer matrices that have been widely used in the nanocomposite design include poly(vinyl alcohol), styrene–butadiene rubber, epoxy resins, polyethylene, polyurethanes, polyamides and polyimides, etc. [5–10]. Different types of nanofillers (including ceramic and metallic nanopowders, nano-clay, carbon nanotubes (CNTs) and nano-$SiO_2$, etc.) have been used to reinforce the polymer matrix [11–14]. Attapulgite is a natural hydrated magnesium–aluminium silicate clay consisting of a three-dimensional network of densely packed rods with a diameter less than 100 nm and a length ranging from hundreds of nanometers to several micrometers for each single rod [15,16].

Shape-memory polymers (SMPs) have the capability of recovering their shape upon application of external stimulus such as thermal treatment or joule heating, light, or chemicals [17–21]. The mechanism of shape recovery in the SMPs can be attributed to 'shrinkage' or movements of polymer chains above either a melting or glass transition temperature [22]. The advantages of SMPs over other shape memory (SM) materials (in particular shape-memory alloys) include their lower cost, low density, high shape recoverability (up to 400%), and easy processability [23,24]. One disadvantage of SMPs is their low stiffness and strength compared to shape-memory alloys or ceramics. Therefore, a rising number of studies currently search for nano-size fillers to enhance the mechanical and shape-memory recovery properties of SMPs [25–28]. In this paper, attapulgite has been used to enhance the mechanical properties of polyurethane (PU), one of the most commonly used SMPs. We find that pre-treatment

---

* Corresponding author. Tel.: +44 0131 4514381.
  E-mail address: R.Y.Fu@hw.ac.uk (Y.Q. Fu).

of attapulgite powder has a dramatic influence on the mechanical, thermal and shape-memory properties of the PU matrix nanocomposite.

## 2. Experimental

Commercial polyurethane MM5520 pellets from Mitsubishi Heavy Industries and attapulgite clay nanoparticles, $(Mg,Al)_2Si_4O_{10}(OH)\cdot4(H_2O)$ were used in this study. Some of the attapulgite clay powder was heat-treated in an oven (in air) at 850 °C for 2 h. A Haake Rheocord 90 Torque Mixer was used for the mechanical mixing of the PU and attapulgite powders at 200 °C, and the SMP nanocomposite samples were prepared by a hot press. More information can be found in Ref. [29].

Scanning electron microscopy (SEM, Philips XL30-FEG) and high resolution transmission electron microscopy (HR-TEM, JEOL 2010F operating at 200 kV) were used to study the morphology of the attapulgite powders. The powder samples were dispersed in isopropanol in an ultrasonic bath for 10 min before SEM and TEM observations. A Fourier transform infrared spectrometer (Satellite FTIR Spectrometer, Mattson) was used to detect the absorption peaks of untreated and thermally treated attapulgite powders. The samples were prepared using the KBr pellet technique. Thermogravimetric analysis (TGA) of the commercial clay powder was carried out using a TA Instrument TGA 2950, and a 5 mg sample was heated in an alumina crucible with a heating rate of 10 °C/min from room temperature to 900 °C under $N_2$ atmosphere. Differential scanning calorimetry (DSC) analyses were performed with a Thermal Advantage DSC 2010 at a heating rate of 10 °C/min under a constant nitrogen flow. Microhardness (Vickers) testing was performed on the SMP and nanocomposite samples with average hardness readings calculated from at least five indentation tests. The indentation loads were varied between 98 to 980 mN and the indentation time was fixed at 20 s. The temperature dependence of hardness of SMP nanocomposite samples was tested using a Peltier heater beneath the composites. A profilometer (DEKTAK 3) was used for scanning the profile of the indents during shape recovery by heating.

## 3. Results and discussions

### 3.1. Clay powder analysis

Fig. 1 shows an SEM image of the commercial attapulgite clay powder revealing a loose fiber bundle structure. The length of each fiber varies from submicrometer to few micrometers and the diameter is about tens of nanometers. The TEM micrograph in Fig. 2a shows that the commercial attapulgite particles are highly dispersed individual rod-like, without any aggregations. Selected area electron diffraction (SAED, not shown) reveals its amorphous nature, confirmed by the HR-TEM image in Fig. 2b and c. The diameter of individual fibers is about 20–50 nm, whereas the average length is a few micron. The mean value of the aspect ratios of the fibers ($L/d$) is in the range of 40–100.
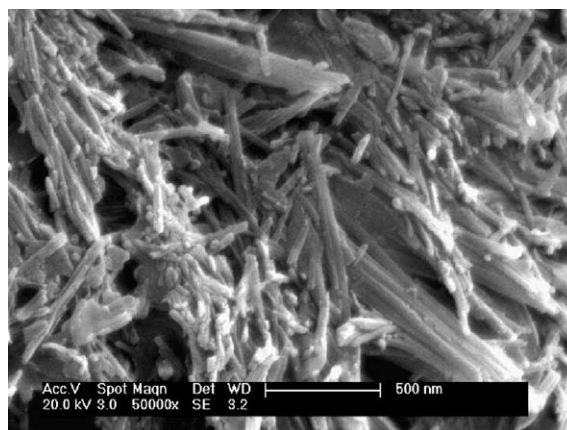


**Fig. 1.** SEM observation of the commercial clay revealing a loose fiber bundle structure, with the length of fibers varying from submicrometer to few micrometers and the diameter about tens of nanometer.

After heat treatment, the attapulgite fibers reconstruct and combine together to form a bundled structure (see Fig. 3a), which could no longer be broken even by ultrasonication for an extended time. The ring-like scattered diffraction spots reveal the nanocrystalline feature as shown by the inset SAED pattern of Fig. 3a. The corresponding HR-TEM images in Fig. 3b and c confirm this new feature. Individual crystallites are embedded in the amorphous matrix with a separation of around 5 nm.

Fig. 4 shows the FTIR results of the commercial and heat-treated attapulgite powders. There are two types of molecules containing hydroxyl groups associated with the natural attapulgite. The peak at 3430 cm$^{-1}$ corresponds to the hydroxyl stretching vibrations of absorbed moisture [30]. Absorbance peak at 3552 cm$^{-1}$ can be attributed to the anti-symmetric stretching modes of molecular water coordinated with the magnesium at the edges of the channel [31]. The peak at 1654 cm$^{-1}$ is associated with the hydroxyl deformation mode of zeolitic water, and the peak at 984 cm$^{-1}$ with the bending vibration of —OH group [32].

In comparison with the spectrum of the commercial attapulgite powder, the FTIR spectrum of the heat-treated clay revealed a broadening of the peak at 3436 cm$^{-1}$, whereas the 1654 cm$^{-1}$ mode was lost. This suggests that heat treatment had removed most inter-fibrillar water, and reduced most of the —OH group content in attapulgite. As shown in Fig. 4, the decrease in —OH group content led to absorbance peaks at 1074 and 984 cm$^{-1}$ which can be attributed to the symmetric and anti-symmetric Si—O—Si stretching vibrations [33,34]. The peak at 800 cm$^{-1}$ indicates the presence of Si—O—Al and O—Al bonds [34]. It should be pointed out that the peak at 3436 cm$^{-1}$ is still pronounced but shifted from 3430 cm$^{-1}$ after the heat treatment. This is due to the O—H stretch formed after removing the inter-fibrillar water [35].

The TGA result of the commercial powder is shown in Fig. 5 and reveals a three-stage change during heating. The first stage at a temperature of about 100 °C corresponds to the loss of moisture which may exist in attapulgite powder as the free water. The second stage

MACROMOLECULAR NANOTECHNOLOGY
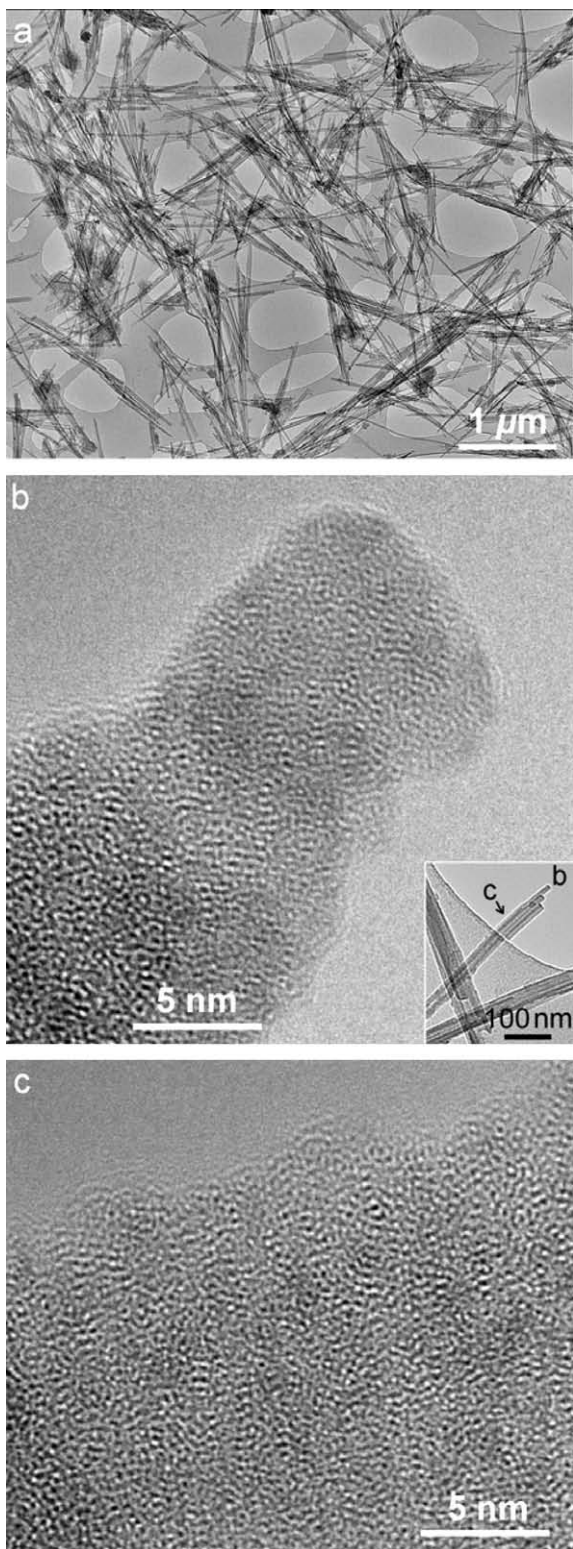


**Fig. 2.** TEM observation of non-treated clay powder: (a) overview, (b) and (c) HR-TEM micrographs taken at the end and body of a clay fiber indicated in the inset.
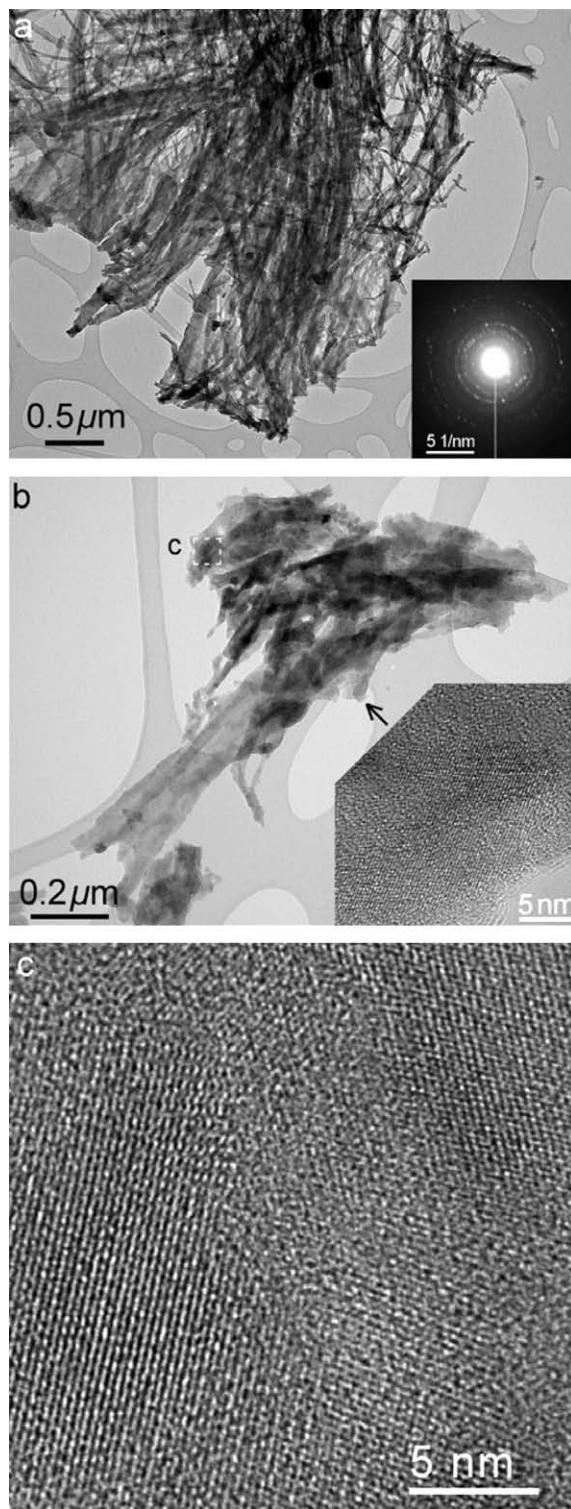


**Fig. 3.** TEM observation of heat-treated clay powder: (a) overview and electron diffraction pattern, (b) and (c) HR-TEM micrographs taken at the indicated position of a clay cluster.
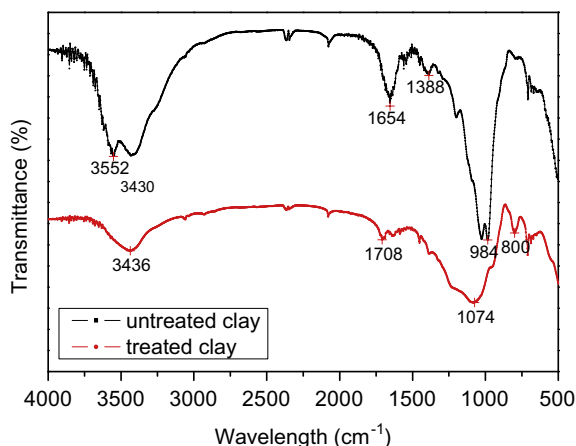
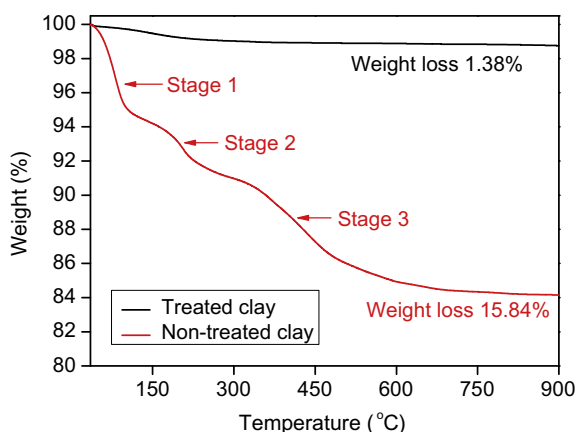**Fig. 4.** FTIR analysis of commercial and heat-treated clay powders.



**Fig. 5.** TGA analysis of clay powders showing the weight loss during heating for both the commercial and heat-treated clay powders.

occurs at about 200 °C when the zeolitic tube is destroyed, coinciding with the loss of hygroscopic water and zeolitic water [36]. The third stage beyond 450 °C when the hydroxyl group is gradually reduced. The total weight loss is close to 15.84%. Compared with commercial clay, the heat-treated one did not show a significant drop in weight (see Fig. 5); even re-adsorption of water molecules after heat treatment is negligible.

In brief, thermal treatment removes water molecules and most hydroxyl groups in the natural clay powders based on the thermal analysis and IR results. The treated clay powders become crystallized and exhibit a bundled structure as shown in TEM.

### 3.2. Hardness results

#### 3.2.1. Hardness vs. load and heat treatment of clay powder

Fig. 6 shows the microhardness data of the pure PU, treated and untreated clay reinforced composites as a function of applied normal load. Hardness of the PU-based shape-memory materials decreases as a function of
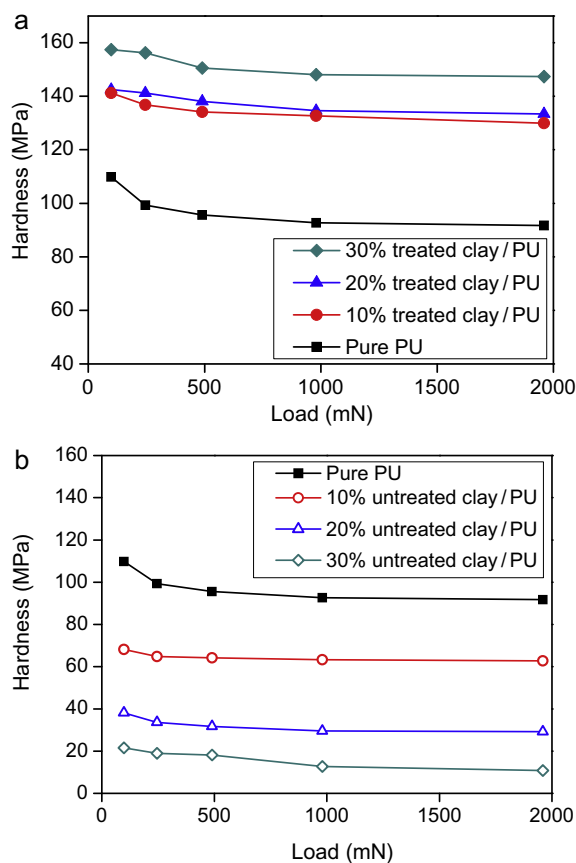


**Fig. 6.** Hardness of pure PU and PU-based shape-memory composites reinforced with (a) treated and (b) untreated clay powders.

indentation load, especially at small loads. For ductile materials such as metals, hardness normally decreases with increasing indentation load, which is commonly called indentation size effect (ISE) [37–39]. Several explanations have been used to explain the origin of the ISE, including limitations in experimental conditions (low resolution of the objective lens, work hardening or softening generated during the surface preparation, intrinsic structural factors of the material, such as work hardening during indentation, indentation elastic recovery and grain size effect) [40–42]. The pure PU sample shows the most significant decrease in hardness as a function of normal load (see Fig. 6). This might be explained by the apparent elastic recovery of PU, which could "artificially" enhance the microhardness value at a low load due to shrinkage of the indentations. At a high load, this artificial enhancing effect is not significant as the indention is quite large.

Fig. 7 summarizes the averaged hardness of the PU-based shape-memory composites as a function of the content of heat-treated and untreated clay, measured at different indentation loads as indicated in Fig. 6. Both Figs. 6 and 7 clearly show that, with addition of the heat-treated clay powder, the hardness of the composites significantly increases with the content of the clay powders. At 30 wt.% content of the treated clay powder, the microhardness reaches a maximum value of about 160 MPa, which is
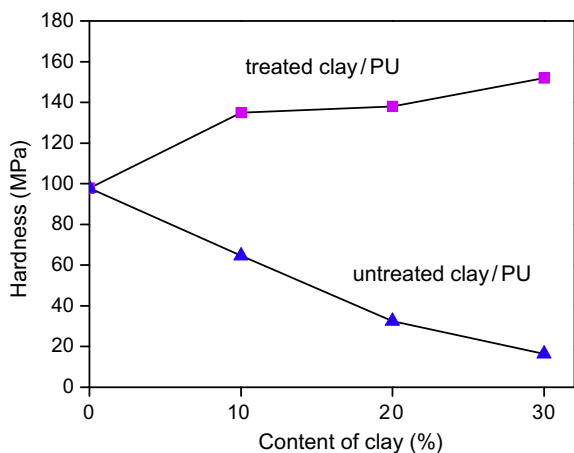
MACROMOLECULAR NANOTECHNOLOGY

**Fig. 7.** Averaged hardness of PU-based shape-memory composites as a function of the content of untreated and treated clay powders.



**Fig. 9.** Microhardness of PU-based shape-memory composites vs. temperature.

nearly a 60% improvement compared to that of the pure PU. On the contrary, adding untreated clay powder results in a tremendous decrease in hardness of the nanocomposites of up to nearly 85% at 30 wt.% content of untreated clay powder.

The DSC traces of the pure PU and the PU-based nanocomposites are shown in Fig. 8. The glass transition temperature ($T_g$) is evident by a step in the DSC trace. The $T_g$ of the nanocomposites decreases upon addition of the untreated clay powder, but not when the heat-treated clay is incorporated. We attribute this decrease in $T_g$ to the presence of moisture and excessive hydroxyl and other organic groups which exist in the non-treated clay powders and make it harder to obtain a good interfacial bonding between polymer and nanofiller. Moisture also acts as plasticizer for the PU polymer causing the decrease in both the $T_g$ and the strength of the polymer [40,41]. Because the $T_g$ of the nanocomposites with the non-treated clay powder decreases below room temperature, the materials becomes very soft during testing.
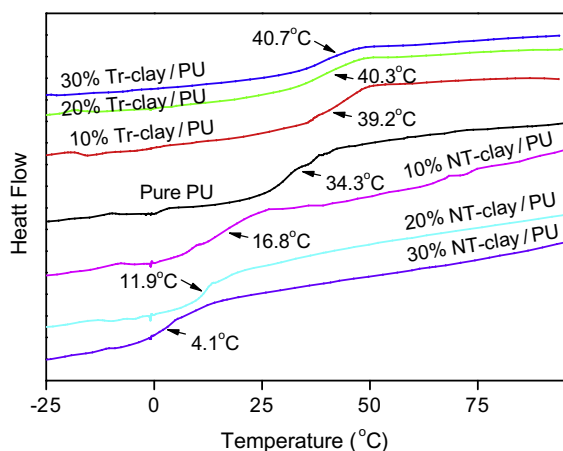
In contrast, addition of the heat-treated nano-clay leads to an increase in the $T_g$ of the nanocomposites by 5 °C compared to the pure PU. In the absence of a plasticizer, the addition of the nanofiller leads to restricted segmental motion of the polymer chains which raises the $T_g$ [42,43].

### 3.2.2. Hardness vs. temperature

Fig. 9 shows the hardness data of PU and treated clay nanocomposites as a function of temperature. Here the logarithm of microhardness, ln $H_v$, is plotted against the temperature $T$ to show the changes in hardness value. The hardness value was found to decrease with temperature in the hybrid composite following the exponential law reported in references [44,45], for the semi-crystalline or amorphous polymer:

$$H_v = H_{vo} \times \exp(-\beta T) \tag{1}$$

where $H_{vo}$ is the hardness of the material at 0 K and $\beta$ is the coefficient of thermal softening. Eq. (1) can be changed into:

$$\ln H_v = \ln H_{vo} - \beta T \tag{2}$$

From Fig. 9, the ln ($H_v$) value decreases linearly with the temperature for all the samples. However, there is an apparent discontinuity of the thermal expansion coefficient around $T_g$, although it becomes less apparent with increasing the clay content. It implies that the microhardness test at different temperatures can be used as a tool to determine the $T_g$ of the polymer and its nanocomposites. A continuous increase in $T_g$ with filler content is also evident from Fig. 9, which supports the DSC results in Fig. 8.

### 3.3. Shape recovery

The shape recovery of the indentation marks was tested using a Peltier heater with a maximum temperature kept below 50 °C. Figs. 10 and 11 show the changes of the indentations at different temperatures for the pure PU and a PU nanocomposites containing 20 wt.% treated clay, respectively. The indentations gradually disappear upon



**Fig. 8.** DSC analysis result of PU-based shape-memory composites with the glass temperature indicated for each composite.

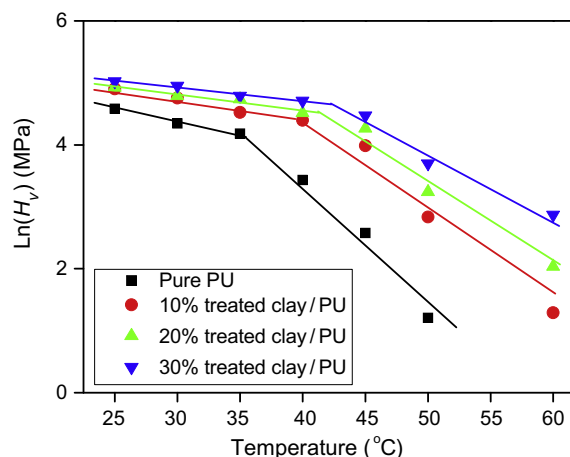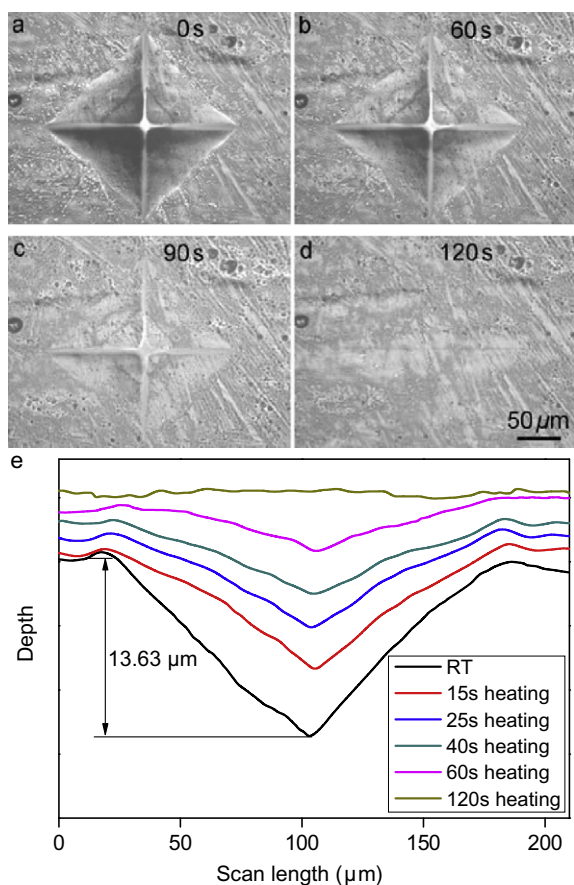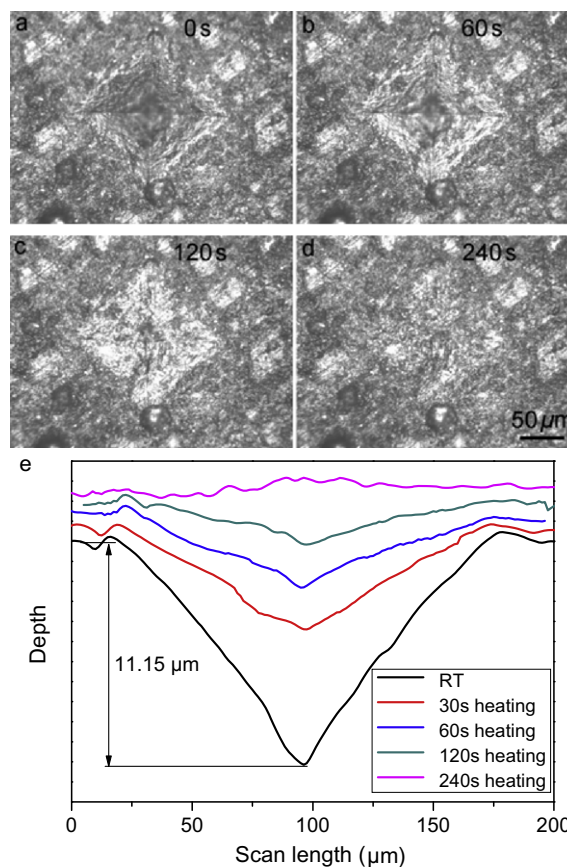MACROMOLECULAR NANOTECHNOLOGY

Fig. 10. OM micrographs showing the evolution of the indentation on pure PU during heating at 50 °C for different time: (a) 0, (b) 60, (c) 90 and (d) 120 s. (e) Profile evolution of the indentation heated for different times indicated.



Fig. 11. OM micrographs showing the evolution of the indentation on 20% treated clay/PU composite during heating at 50 °C for different time: (a) 0, (b) 60, (c) 120 and (d) 240 s. (e) Profile evolution of the indentation heated for different times indicated.

heating, indicating a good self-healing performance. Figs. 10(e) and 11(e) also show the cross-section profiles of the indentations of these two samples. Prior to heating, the pile-up of the indentations can be clearly observed, indicating the significant plastic deformation nature of the SMP and nanocomposites [46]. The nanocomposite samples are found to have a slower recovery speed than those of the PU under the same temperature.

## 4. Discussions

From the above results, it is confirmed that the mechanical and thermal properties of PU-based shape-memory nanocomposites significantly depend on the pre-treatment of the nanopowders. After heat treatment of the clay nanopowders, FTIR and TGA results revealed the removal of moisture and most hydroxyl groups from the clay. The presence of moisture in the untreated clay had a significant plasticization effect and thus deteriorated the mechanical properties [41,42]. In this paper, less than 4% moisture could result in nearly 85% decrease in hardness, regardless of the enhancement brought by clay. TEM observations confirmed the formation of a crystallized and bundled fiber structure

after heat treatment. These changes correlate with the improved interfacial properties of the nanofillers, thus enhancing the mechanical properties of the nanocomposites. The results clearly show that pre-treatment of the nanofiller is crucial for the good performance of the nanocomposites, and drying of PU/untreated attapulgite composite could significantly affect its mechanical properties.

Agglomeration of the nano-clay powders is generally significant due to their large surface energy. A simple mechanical mixing using a Haake Mixer was inefficient to disperse and intercalate the nanofillers uniformly inside the SMP, thus a partially separated nanocomposite, the multiphase structure like in Fig. 12a was obtained, which prevented any significant enhancement of mechanical properties for the SMP nanocomposites. A possible solution is to use a pre-surface treatment method for the nanofillers by physical (e.g. treatment with surfactant) or chemical methods (reaction with coupling agent or surface grafting of a polymer), which could remove the moisture and separate the nanofillers more effectively [47]. Therefore, surface energy would be reduced and embedding structure could be intercalated with nanofillers resulting in well ordered cluster morphology as illustrated in Fig. 12b. The

MACROMOLECULAR NANOTECHNOLOGY
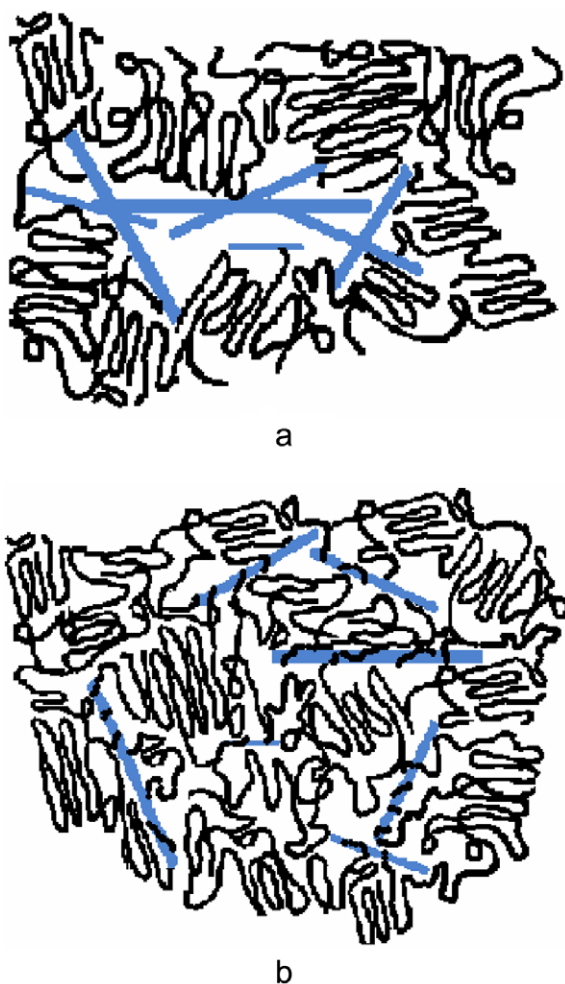


**Fig. 12.** Scheme of nanocomposite arising from the interaction of layered silicates and polymers: (a) conventional composites phase separated and (b) exfoliated nanocomposites.

nanocomposites are broken down into nanoscale building blocks which disperse the nano-clay fibers completely and uniformly. The surface chemical pre-treatment of the nano-clay particles is essential for the further improvement of the mechanical properties of the nanocomposites.

## 5. Conclusion

Mechanical properties of the attapulgite clay reinforced polyurethane shape-memory nanocomposites are strongly dependent on the pre-treatment of the nanopowders. Following heating treatment of the nano-powders, the loss of moisture and most surface hydroxyl groups provided a crystallized and bundled structure. Improved interfacial bonding between the polymer and filler interface enhanced the mechanical properties of the nanocomposites. In comparison, untreated PU–clay nanocomposites showed a decrease in both the $T_g$ and the strength of the nanocomposites. PU-based composites containing 30 wt.% treated clay nanoparticles exhibited the same capability of shape recovery as pure PU although recovery speed was slightly slower.

## References

[1] Schmidt D, Shah D, Giannelis EP. New advances in polymer/layered silicate nanocomposites. Curr Opin Solid State Mater Sci 2002;6(3):205–12.
[2] Schmidt G, Malwitz MM. Properties of polymer–nanoparticle composites. Curr Opin Colloid Interface Sci 2003;8(1):103–8.
[3] Sanchez C, Lebeau B, et al. Optical properties of functional hybrid organic–inorganic nanocomposites. Adv Mater 2003;15(23):1969–94.
[4] Morgan AB. Flame retarded polymer layered silicate nanocomposites: a review of commercial and open literature systems. Polym Adv Technol 2006;17(4):206–17.
[5] Tobushi H, Hayashi S, Hoshio K, Miwa N. Influence of strain-holding conditions on shape recovery and secondary-shape forming in polyurethane-shape memory polymer. Smart Mater Struct 2006;15:1033–8.
[6] Kawasumi M, Hasegawa N, Kato M, Okada A. Preparation and mechanical properties of polypropylene–clay hybrids. Macromolecules 1997;30:6333–8.
[7] Peng ZQ, Chen DJ. Study on the nonisothermal crystallization behavior of poly(vinyl alcohol)/attapulgite nanocomposites by DSC analysis. J Polym Sci B Polym Phys 2006;44(3):534–40.
[8] Tian M, Qu CD, Feng YX. Structure and properties of fibrillar silicate/SBR composites by direct blend process. J Mater Sci 2003;38(24):4917–24.
[9] Shen L, Lin YJ, Du QG, Zhong W, Yang YL. Preparation and rheology of polyamide-6/attapulgite nanocomposites and studies on their percolated structure. Polymer 2005;46(15):5758–66.
[10] Lai SQ, Yue L, Li TS, Liu XJ, Lv RG. An investigation of friction and wear behaviors of polyimide/attapulgite hybrid materials. Macromol Mater Eng 2005;290(3):195–201.
[11] Utracki LA. Polymeric nanocomposites: compounding and performance. J Nanosci Nanotechnol 2008;8:1582–96.
[12] Carrado KA. Synthetic organo- and polymer-clays: preparation, characterization, and materials applications. Appl Clay Sci 2000;17(1–2):1–23.
[13] Hussain F, Hojjati M, Okamoto M, et al. Review article: polymer–matrix nanocomposites, processing, manufacturing, and application: an overview. J Comp Mater 2006;40(17):1511–75.
[14] Carastan DJ, Demarquette NR. Polystyrene/clay nanocomposites. Int Mater Rev 2007;52(6):345–80.
[15] Pan Hongxia, Chen Dajun. Preparation and characterization of waterborne polyurethane/attapulgite nanocomposites. Eur Polym J 2007;43(9):3766–72.
[16] Bradley WF. The structures, scheme of attapulgite. Am Miner 1940;25:405–10.
[17] Lendlein A, Kelch S. Shape memory polymers. Mater Today 2007;10:20–9.
[18] Kim BK, Lee SY, Xu M. Polyurethanes having shape memory effects. Polymer 1996;37(26):5781–93.
[19] Baer G, Wilson TS, et al. Shape-memory behavior of thermally stimulated polyurethane for medical applications. J Appl Polym Sci 2006;103(6):3882–92.
[20] Lendlein A, Jiang H. Light-induced shape-memory polymers. Nature 2005;434:879–82.
[21] Mohr R, Kratz K, et al. Initiation of shape-memory effect by inductive heating of magnetic nanoparticles in thermoplastic polymers. PNAS 2006;103(10):3540–5.
[22] Lendlein Andreas, Langer Robert. Biodegradable, elastic shape-memory polymers for potential biomedical applications. Science 2002;296:1673–76.

[23] Hayashi S, Kondo S, Kapadia P, Ushioda E. Room-temperature functional shape-memory polymers. Plast Eng 1995;51(22):29–31.

[24] Liang C, Rogers CA, Malafeew E. Investigation of shape memory polymers and their hybrid composites. J Int Mater Syst Struct 1997;8(4):380–6.

[25] Gunes IS, Jana SC. Shape memory polymers and their nanocomposites: a review of science and technology of new multifunctional materials. J Nanosci Nanotechnol 2008;8(4):1616–37.

[26] Gall K, Dunn ML, Liu Y, Finch D, Lake M, Munshi NA. Shape memory polymer nanocomposites. Acta Mater 2002;50(20):5115–26.

[27] Gunes IS, Cao F, Jana SC. Evaluation of nanoparticulate fillers for development of shape memory polyurethane nanocomposites. Polymer 2008;49(9):2223–34.

[28] Cho JW, Lee SH. Influence of silica on shape memory effect and mechanical properties of polyurethane–silica hybrids. Eur Polym J 2004;40(7):1343–8.

[29] Pan GH, Huang WM, Ng ZC, Liu N, Phee SJ. Glass transition temperature of polyurethane shape memory polymer reinforced with treated/non-treated attapulgite (playgorskite) clay in dry and wet conditions. Smart Mater Struct 2008;17:045007.

[30] Frost Ray L, Cash Gerg A, Kloprogge Theo J. Rocky Mountain leather', sepiolite and attapulgite—an infrared emission spectroscopic study. Vib Spectrosc 1998;16(2):173–84.

[31] Frost Ray L, Locos O1iver B, Ruan Huada, et al. Near-infrared and mid-infrared spectroscopic study of sepiolites and palygorskites. Vib Spectrosc 2001;27(1):1–13.

[32] Farmer VC, editor. Infrared spectra of minerals. London (GB): London Mineralogical Society; 1974. p. 331-63.

[33] Suárez M, García-Romero E. FTIR spectroscopic study of palygorskite: influence of the composition of the octahedral sheet. Appl Clay Sci 2006;31(1–2):154–63.

[34] Augusburger MS, Strasser E, et al. FTIR and Mossbauer investigation of a substituted palygorskite: silicate with a channel structure. J Phys Chem Solids 1998;59(2):175–80.

[35] Araújo Melo DM, Ruiz JAC, et al. Preparation and characterization of terbium palygorskite clay as acid catalyst. Micropor Mesopor Mater 2000;38(2–3):345–9.

[36] Frost RL, Ding Z. Controlled rate thermal analysis and differential scanning calorimetry of sepiolites and palygorskites. Thermochim Acta 2003;397(1–2):119–28.

[37] Manika E, Maniks J. Size effects in micro- and nanoscale indentation. Acta Mater 2006;54(8):2049–56.

[38] Gao YX, Fan H. A micro-mechanism based analysis for size-dependent indentation hardness. J Mater Sci 2002;37(20):4493–8.

[39] Iost A, Bigot R. Indentation size effect: reality or artefact? J Mater Sci 1996;31(13):3573–7.

[40] Yang B, Huang WM, et al. Effects of moisture on the glass transition temperature of polyurethane shape memory polymer filled with nano-carbon powder. Eur Polym J 2005;41(5):1123–8.

[41] Yang B, Huang WM, et al. Effects of moisture on the thermomechanical properties of a polyurethane shape memory polymer. Polymer 2006;47(4):1348–56.

[42] Lu H, Shen H, et al. Rod-like silicate–epoxy nanocomposites. Macromol Rapid Commun 2005;26(18):1445–50.

[43] Choi YS, Choi MH, et al. Synthesis of exfoliated PMMA/Na-MMT nanocomposites via soap-free emulsion polymerization. Macromolecules 2001;34:8978–85.

[44] Kajaks J, Flores A, et al. Crystallization kinetics of poly(ethylene naphthalene-2,6-dicarboxylate) as revealed by microhardness. Polymer 2000;41(21):7769–72.

[45] Ania F, Martinez-Salzar J, Balta Calleja FJ. Physical ageing and glass transition in amorphous polymers as revealed by microhardness. J Mater Sci 1989;24(8):2934–8.

[46] Su JF, Huang WM, Hong MH. Indentation and two-way shape-memory in a NiTi polycrystalline shape-memory alloy. Smart Mater Struct 2007;16:137–44.

[47] Chattopadhyay DK, Raju K. Structural engineering of polyurethane coatings for high performance applications. Prog Polym Sci 2007;32(3):352–418.

MACROMOLECULAR NANOTECHNOLOGY